Image Segmentation for Hexagonally Sampled Images Using Statistical Region Merging

Xiqiang Zheng School of Science, Technology, Health and Humen Services Voorhees University, Denmark, SC 29042, USA xzheng@yoorhees.edu

Abstract— The statistical region merging (SRM) method for image segmentation is based on some solid probabilistic and statistical principles. It produces good segmentation results, and is efficient in term of the computational time. The original SRM algorithm is for Cartesian images sampled by square lattices (sqL). Because hexagonal lattices (hexL) have the advantage that each lattice point in a hexL has six equidistant adjacent lattice points, in this paper, we perform image segmentation for hexagonally sampled images using SRM. We first convert the SRM algorithm from sqLs to hexLs. Then we use some test images to compare the corresponding segmentation effect for hexLs versus sqLs. The experimental results have shown that a hexL exhibits evidently better image segmentation effect than the corresponding sqL (with the same spatial sampling rate as the hexL) using the usual 4-connectivity. Finally, we point out that CT image segmentation may benefit from using hexLs since they provide better image reconstruction effect than sqLs.

Keywords— Image segmentation, hexagonal lattices, statistical region merging

I. INTRODUCTION

Image segmentation is to divide a digital image into some homogeneous groups or regions such that the features within each region vary little and the feature difference on the adjacent regions should be as big as possible. It can be applied to image analysis in fields such as medical imaging studied in [1] by Sharma and Aggarwal and in [2] by Windisch and Kozlovszky.

As shown in [3] by Nija et al., the statistical region merging (SRM) method in [4] by Nock and Nielsen is an effective image segmentation method. By Schindler and Suter [5], SRM produces good segmentation results and is very efficient in terms of computational time. Furthermore, each segment produced by SRM is a connected component with respect to the connectivity for the SRM segmentation method, and hence the size of each component can be output immediately from the SRM segmentation. Thus, SRM is used in many situations studied in papers such as [6-12].

The advantages of hexagonal lattices (hexL) for image processing and for application domains such as computerized tomography (CT) imaging are shown in papers such as [13-20]. As shown in [21], each lattice point in a hexL has six equidistant neighbors. Because the adjacency of the lattice points is important for image segmentation, hexLs may produce good image segmentation effects. For CT imaging, by [13,15,16], hexLs produce better image reconstruction effect than the usual

This research is supported by a National Science Foundation grant of the USA with the Federal Award ID Number 2000158.

sqLs. Therefore, hexLs may perform better than sqLs on CT image segmentation.

Wei et al. [17] implemented the graph-cut algorithm (GCA) in [22] for image segmentation on hexLs. Felzenszwalb and Huttenlocher in [23] pointed out that GCA is too slow. When an image size is big, the image segmentation using GCA is not practical. Although the interactive GCA using object and background marking may achieve better effect, the segmentation results may not be good because the geometry of the object may be complicated. But, SRM can handle many situations well, and is convenient to perform image segmentation. In the following, we implement the SRM algorithm on hexLs, and compare them with sqLs for the image segmentation effect.

II. SRM FOR BOTH SQUARE AND HEXAGONAL LATTICES

A. Review of the General SRM Method

The graph building and the region growing (merging) procedures between SRM and the graph-based image segmentation method in [23] are the same. The main difference is the merging criteria. As in [4], an image h to be segmented is taken as an observation of a perfect image h^* . There exist two positive integers Q and g such that, for any pixel of h^* , each color channel of h^* is represented by Q independent random variables that take values in the interval $(\mathcal{O}_{G \circ f}^{\underline{g}})$. The value of g corresponds to the Red-Green-Blue (RGB) values of the image h and is usually set to 256.

As in the usual set notation, for any discretized region R in the domain of the image h, let /R/ denote the cardinal number of the set R. For each color band, let R^- denote the observed average of the color band and let $E(R^-)$ denote the expectation. Consider two such regions R and R^r . By Corollary 1 in [4], for any $0 < o \le 1$, the probability of the event represented by the following inequality is not more than o.

$$|(R^- - R^-) - E(R^- - R^-)| \ge g \frac{1}{2Q} \frac{1}{|R|} + \frac{1}{|R'|} \frac{2}{o}$$

When $E(R^{-}) = E(-R^{-})$, this inequality becomes

$$|R^- - R^-| \ge g \frac{1}{2Q} \frac{1}{|R|} + \frac{1}{|R|} \frac{2}{o}$$

In the actual implementation, let $o = \frac{1}{6/1!^2}$. The two regions R and R^r can be merged only if the above inequality is false.

B. The SRM Method on sqLs

A usual color image h sampled on a sqL is represented as a 3D matrix or array

$$IUh_{i,i,k}: 1 \le i \le m, 1 \le j \le , 1 \le 6 \le 3$$
%.

As shown on the right side of Figure 1 in [21], the pixels of the image h correspond to the lattice points in a sqL. In [4] and [6], 4-connectivity is used for the image segmentation using SRM. An adjacent pair of pixels is called an *edge* of the image h. Let V be the set consisting of the pixels (lattice points); let E be the set of edges; and let G = (V, E) be the corresponding graph. For any such pair of pixels P and Q, the *weight of the corresponding edge* is defined to be

$$maxIU/P_a - Q_a/: a \in \{2,2,2\}$$
 $\circ O \circ$

where P_a denotes a color value at pixel P.

We also considered Sobel filters with kernels of size 3×3 for the computation of the weight of an edge. Let h_a be the a color channel of the image h. The Sobel derivative at a pixel (i, j) of the image h in the horizontal direction is denoted as $Sob_x(i, j)$, and defined to be

$$\frac{1}{2} [2 \cdot h \quad (i+1,j) - 2 \cdot h \quad (i-1,j) + h \quad (i+1,j+1) - h_{a}(i-1,j+1) + h_{a}(i+1,j-1) - h_{a}(i-1,j-1)]$$

The left derivative is denoted as $D_L(i, j)$, and defined to be $h_a(i + 1, j) - h_a(i, j)$; the right derivative is denoted as $D_R(i, j)$, and defined to be $h_a(i, j) - h_a(i - 1, j)$.

If an edge is horizontal with end points (i, j) and (i + 1, j), then the edge weights for Alg. 1 in this paper are based on the weighted absolute values of the Sobel derivatives, the left derivatives and the right derivatives. Let $W_1 \in [0, 1]$ be the weight of $Sob_x(i, j)$. The edge weight is defined to be

$$W_1 \cdot |Sob_x(i,j)| + (1 - W_1) \cdot \frac{1}{2} [|D_R(i,j)| + |D_{\prec}(i,j)|]$$

If an edge is vertical, then the weight can be defined similarly. If an edge is in the diagonal direction with end points (i, j) and (i + 1, j + 1), then the Sobel derivative at the pixel (i, j) in this direction is defined to be

$$\frac{1}{6\sqrt{2}}[2 \cdot h_a(i+1,j+1) - 2 \cdot h_a(i-1,j-1) + h_a(i,j+1) - h_a(i-1,j) + h_a(i+1,j) - h_a(i,j-1)]$$

Similar to $D_R(i,j)$ and $D_L(i,j)$, we can compute the directional

derivatives in two different directions along this diagonal. Then the weight for this edge as well as the edges in another diagonal direction can be similarly computed as in the horizontal direction. If $W_1 = 1$, then the edge weight is the same as the absolute value of the Sobel derivative.

After the weighted graph G is constructed, the SRM method for image segmentation on a sqL can proceed using the following Alg. 1. To compare the SRM based image

segmentation effect using hexLs versus sqLs, we have made Alg. 1 to include the situation of 8-connectivity.

	m 1 Image segmentation using SRM on a sqL with vity $c \in \{4, 8\}$
Input	An image h of size m by by 3, the minimal size, the values of Q and g , and the weight $W_1 \in [0, 1]$ for the directional derivatives using Sobel operators
Step 1	Create a matrix $A = \bigcap a_{i,j} (OO)$ of size m by n such that $a_{i,j} = m(j-1) + i$, which is a 1-to-1 function mapping image pixels to counting numbers from 1 to m ; use the 4-connectivity (8-connectivity respectively) to construct the edge set E and compute the edge weights based on the Sobel directional derivatives, the usual sided directional derivatives, and the value of W_t ; and construct the graph $G = (V, E)$
Step 2	Based on the mapping, vertices of G are denoted as v_k for $k = 1, 2,, V $; let $C_k = \{v_k\}$; and let $C = \{C_k \delta = 1, 2,, V \}$ be the set of components to be merged
Step 3	Sort the elements of E into e_1 , e_2 ,, $e_{ E }$ in non-decreasing edge weights
Step 4	For $q = 1, 2,, E $, let u and v be the two vertices connected by the edge e_q . If the component containing u and the component containing v satisfy the merge criteria, then merge them, compute the average values of the new component, let the index of the bigger component to be the index of the merged component, and map those two indices to the index of the merged component
Step 5	Use the averaged values of the merged components and the map function to construct the segmented image denoted as h_s
Output	The segmented image h_s , the number of classes (segments) in h_s , the number $ E $ of edges, and the number of pixels in each segment

C. The SRM Method on hexLs

As in [20], the image is usually sampled on a sqL, and the area of a Voronoi cell of the lattice is 1. Let R_u be the region that is the union of the Voronoi cells of the lattice points in the image domain. To compare the image segmentation effect of hexLs versus sqLs, we construct a hexL such that the area of a Voronoi cell of the hexL is also 1, which implies that those two lattices

sample the region
$$R_u$$
 with the same sampling rate. Let $_{\rm S} = \sqrt{\frac{2}{\sqrt{3}}}$

and let 0 be the hexL generated by the two vectors $s \cdot [1, 0]$ and $s \cdot [-\frac{1}{2}, \frac{\sqrt{-1}}{2}]$. It is easy to check that the area of a Voronoi cell of 0 is 1. The region R_u may be sampled by the hexL 0 as shown in Fig. 1.

Let Hexhm be an image sampled on the hexL 0. To apply SRM on Hexhm, the lattice points shown in Fig. 1 can be ordered using the left-right and bottom-up order, which generates a 1-to-1 function mapping a counting number i to the ith pixel (lattice point) of Hexhm according to the order. Let N_h be the number of lattice points in the image domain of Hexhm; and let A_h and B_h be the vectors of length N_h such that the ith

component of A_h (A_h), respectively) is the X (, Y) respectively) coordinate of the ith lattice point of Hexhm. The vectors A_h and B_h can be used for image interpolations and resampling between the sqL and the hexL, and can be used to compute the edge weights of the graph for Hexhm. Then we can construct the weighted graph G = (V, E) corresponding to Hexhm. The edge set E of this graph consists of edges in the horizontal, 60° , and 120° directions.

Similar to the situations of the edges in the diagonal directions at a lattice point in the sqL, we can compute the edge weights for Hexhm. For example, if an edge is in the horizontal direction with end points denoted as (i, j) and (i + 1, j) as in Fig. 1, then the Sobel derivative at the pixel (i, j) of the image Hexhm is defined to be

$$\frac{1}{6} \begin{bmatrix} 2 \cdot H & (i+1,j) - 2 \cdot H & (i-1,j) + H & (i+1,j+1) - 4 \\ a & a & a \\ H_a(i,j+1) + H(i,j-1) - H_a(i-1,j-1) \end{bmatrix},$$

where *H* denotes *Hexhm*. The SRM based image segmentation for *Hexhm* can proceed using the following Alg. 2.

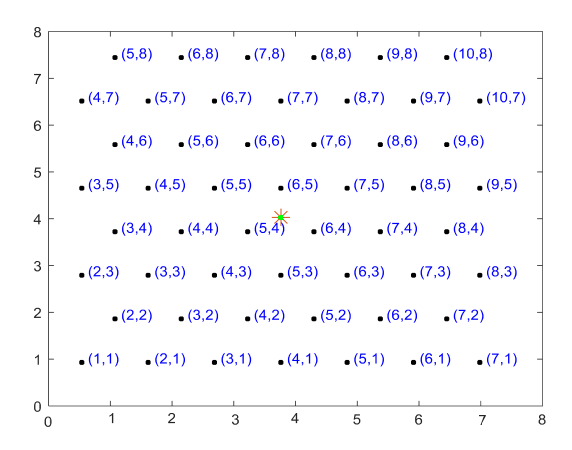


Figure 1: A rectangular region is sampled by a hexL. The red star point denotes the centroid of the region and, for each black lattice point, the numbers inside the parenthesis denote the coordinates in terms of the basis generating the lattice.

Algorithm 2 Image segmentation on a hexL using SRM							
Input	A matrix <i>Hexhm</i> of size <i>Pixels</i> by 3 where <i>Hexhm</i> denotes the image sampled on the pixels in the hexL						
	O as shown in Fig. 1 using the left-right and bottom-up order, the minimal size, the values of Q and g , the weight $W_1 \in [0, 1]$ for the directional derivatives using Sobel operators, and the values of m_{Hex} and m_{Hex} indicating the numbers of rows and columns of the image pixels as in Fig. 1						
Step 1	Generate the hexL O ; by referring to Fig. 1, generate the 1-to-1 function mapping any counting number $i \le P_{ixels}$ to the ith pixel of $Hexhm$ according to the left-right and bottom-up order; use the image pixels to construct the edge set E and compute the edge weights based on the Sobel directional derivatives, the usual sided directional derivatives, and the value of W_I ; and construct the graph $G = (V, E)$						

Steps 2-4	The same as Steps 2-4 in Alg. 1
Step 5	Use the averaged values of the merged components and the map function to construct the segmented image <i>Hexh</i> _s
Output	The segmented image <i>Hexhs</i> , the number of classes (segments) in <i>Hexhs</i> , the number <i>/E/</i> of edges, and the number of pixels in each segment

III. EXPERIMENTAL RESULTS FOR THE SRM METHODS ON HEXAGONAL LATTICES VERSUS SQUARE ONES

In this section, Algs. 1 and 2 are applied to perform image segmentation and to evaluate the corresponding effect. The input and segmented images are plotted for visual comparisons. Furthermore, we have used some convenient and stable evaluation criteria as follows.

For the input image h of size m by 3, let \bar{h} denote the segmented image. The *mean absolute error* (MAE) of the segmentation is defined as

$$MAE = \frac{1}{mn} \sum_{i=1}^{m} \sum_{j=1}^{n} ||h(i,j,:) - h(i,j,:)||,$$

where the norm can be L_1 or L_2 norm. We have computed the MAE for each norm. As mentioned in [25], the MAE is less sensitive to outliers than the root-mean-square Error. When the number of segments of the segmentation is the same for both algorithms, the algorithm with less MAE values is preferred. In our experiments, we let the minimal size be 3, g = 256, $W_1 = 0.4$, and $Q = 2^k$ for k = 6, 5, ..., 0.

For a usual image sampled on the sqL, to fairly compare the segmentation effect of those two different kinds of lattices, the image is resampled to a certain randomized grid as in [20] by replacing each lattice point $(i, j) \in sqL$ with $(i, j) + (r_1, r_2)$, where r_1 and r_2 are random numbers between -0.45 and 0.45. Then interpolations are used to obtain two images sampled on the sqL and the hexL, respectively. Because of the randomized grid, the computational results may be a bit different for different experiments. But the experimental results are almost consistent for the comparison of image segmentation effect of the hexL versus the sqL. For the input image (from [27]) shown in the top-left of Fig. 2, the segmentation results are shown in

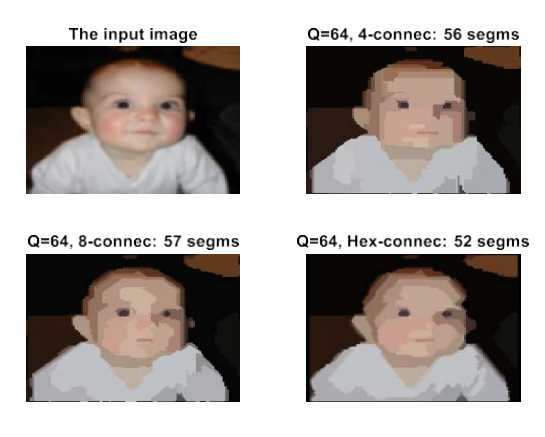


Figure 2: The top-left is the input image for the algorithms gen. images in Figs 2, 3, 4, and 5.



Figure 3: Segmented images using the sqL with 4-connectivity.

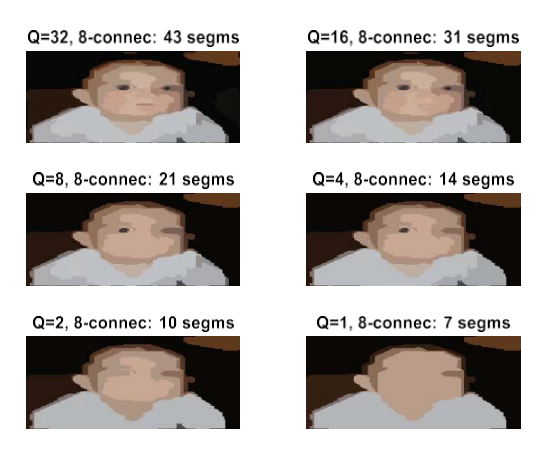


Figure 4: Segmented images using the sqL with 8-connectivity.

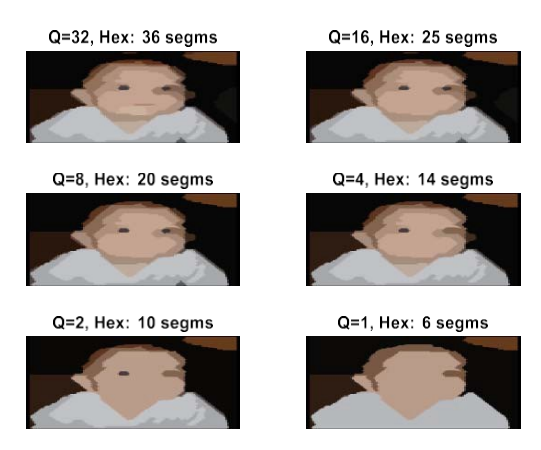


Figure 5: Segmented images using the hexL.

Figs. 2, 3, 4, and 5; and the corresponding MAE values are shown in Tables 1 and 2. From those images, we can see that the

boundaries of the salient objects in the segmented images using the sqL with 4-connectivity tend to be horizontal and vertical, and the salient objects are not quite similar to those in the input image. From Tables 1 and 2, we can see that for each Q value, the MAE values for the hexL are usually smallest.

Table 1: The MAE values for Algs. 1 and 2 using L1 norm with different Q values and connectivity using the input in Fig. 2.

Q	32	16	8	4	2	1
Alg. 1, 4-conne.	26.48	28.43	30.02	33.67	36.54	40.21
Alg. 1, 8-conne.	23.04	24.88	26.62	29.15	32.23	37.11
Alg. 2, hexL.	22.12	23.24	24.76	26.96	30.05	36.39

Table 2: The MAE values for Algs. 1 and 2 using L2 norm with different Q values and connectivity using the input in Fig. 2.

Q	32	16	8	4	2	1
Alg. 1, 4-conne.	15.92	17.07	18.06	20.16	21.86	24.00
Alg. 1, 8-conne.	14.00	15.09	16.16	17.63	19.42	22.29
Alg. 2, hexL.	13.49	14.16	15.04	16.29	18.13	21.76

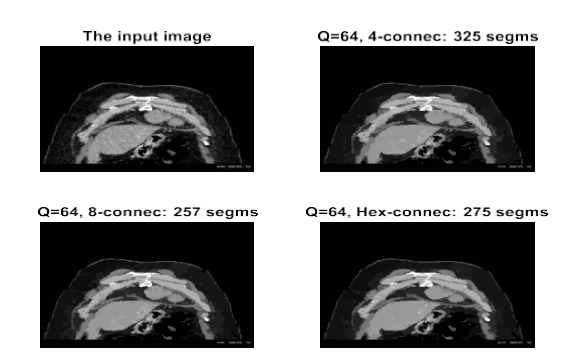
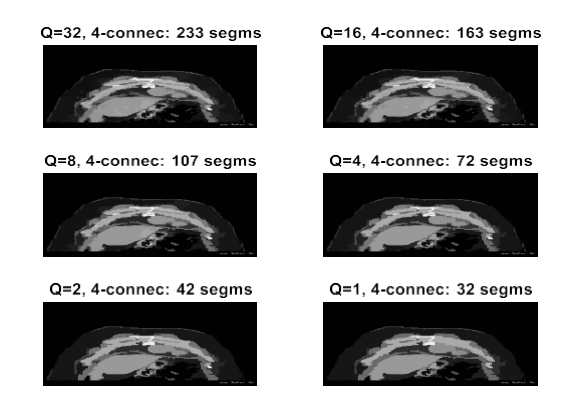


Figure 6: The top-left is the input image for the algorithms generated images in Figs 6, 7, 8, and 9.



Figure~7: Segmented~images~using~the~sqL~with~4-connectivity.

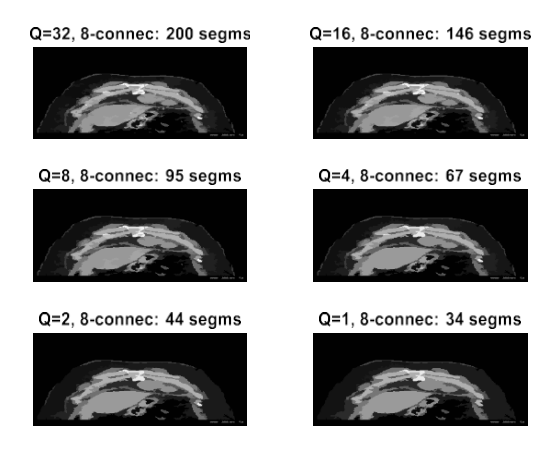


Figure 8: Segmented images using the sqL with 8-connectivity.

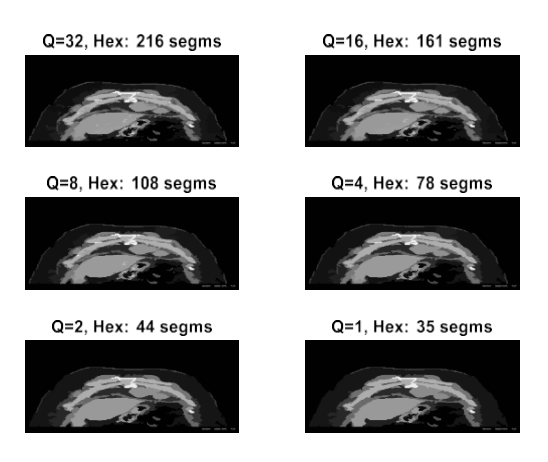


Figure 9: Segmented images using the hexL.

Table 3: The MAE values for Algs. 1 and 2 using L1 norm with different Q values and connectivity using the input in Fig. 6.

Q	32	16	8	4	2	1
Alg. 1, 4-conne.	15.32	15.98	16.84	17.94	19.57	20.58
Alg. 1, 8-conne.	14.44	14.95	15.83	16.66	18.18	19.20
Alg. 2, hexL.	13.75	14.24	15.18	15.94	17.71	18.60

We also used another input image (from [28]) shown in the top-left of Fig. 6. The segmentation results are shown in Figs. 7, 8, and 9; and the corresponding MAE values are shown in Table 3. When Q=64, the input image and segmented images are shown in Fig. 6.

As for the computational time of the SRM algorithm using the hexL, the size of the input image in the top-left of Fig. 2 (, Fig. 6 respectively) is 130 by 132 by 3 (, 630 by 630 by 3 respectively). The computational time by Matlab is shown in Table 4. As the number of edges for the hexagonally sampled images is just about 75% of the number of edges for the corresponding image sampled on the sqL with 8-connectivity, its computational time is much less. In some actual application

domains such as CT imaging, by [13] and [15], the image can be reconstructed directly using the hexL; and the reconstruction effect using the hexL is better than the effect using the sqL. Then the SRM algorithm using the hexL can be directly applied without resampling from the sqL. Although the 2nd input image has size 630 ×630 ×3, the computational time of each algorithm is acceptable. In the future, the display device may also be made for hexLs. Therefore Alg. 2 has promising applications.

Table 4: Computational time in seconds for Algs. 1 and 2.

	•			
Image size	Alg.1 (4-connec.)	Alg.1 (8-connec.)	Alg. 2 (Hex.)	
130 <i>×</i> 132 <i>×</i> 3	0.0245 seconds	0.4965 seconds	0.0372 seconds	
630 <i>×</i> 630 <i>×</i> 3	0.7441 seconds	12.0885 seconds	1.2167 seconds	

IV. CONCLUSION AND FUTURE WORK

We have developed a computer algorithm for the SRM method on the hexL. The algorithm is tested using some images and *Q* values. The experimental results are evaluated using the *MAE* measure. The segmented images are displayed, and the *MAE* values are tabulated for convenient comparisons.

The experimental results have shown that the hexL achieves better image segmentation effect than the sqL with the usual 4-connectivity. For the hexagonally sampled image, although the number of edges is much less than the corresponding number for the image sampled on the sqL with 8-connectivity, the image segmentation effect is still very good. As shown in those segmented images, image segmentation may reduce the amount of noise in the salient features of an image, and may make the boundaries of the salient objects more evident. Furthermore, each segment in the output image of the SRM algorithms is connected, and the size of the segment can be output. The SRM algorithm on the hexL may help automatically determine the sizes of salient objects in an image. Because a lattice is important for efficient indexing of image pixels and for mathematical operations on the image, other sampling schemes are not considered in this paper.

In [29] by Khan, several image segmentation algorithms are surveyed. In the future, we may compare the sqL with the hexL for image segmentation using other efficient algorithms such as those in [30-32] based on watershed transforms, histogram thresholding, etc. Furthermore, we may reconstruct the images using both the sqL and hexL from the same CT sinogram as mentioned in [20]. Then perform image segmentations using Algs. 1 and 2, and compare the effect of those algorithms. We may also generalize the image segmentation algorithms from hexLs to 3-dimensional optimal sampling lattices as in [33].

ACKNOWLEDGMENT

Many thanks to Dr. Song Wang (in Department of Computer Science and Engineering at University of South Carolina) for serving as a consultant of the research project and for his valuable suggestions.

REFERENCES

[1] N. Sharma and L. M. Aggarwal, "Automated medical image segmentation techniques," J. Med. Phys., vol. 35, no. 1, pp. 3-14, 2010.

- [2] G. Windisch and M. Kozlovszky, "Framework for Comparison and Evaluation of Image Segmentation Algorithms for Medical Imaging," IFMBE proceedings, vol. 49, pp. 480-483, 2015.
- [3] K. S. Nija, C. P. Anupama, V. P. Gopi, and V. S. Anitha, "Automated segmentation of optic disc using statistical region merging and morphological operations," Phys Eng Sci Med., vol. 43, no. 3, pp. 857-869, 2020.
- [4] R. Nock and F. Nielsen, "Statistical region merging," IEEE Trans. Pattern Anal. Mach. Intell.. vol. 26, no. 11, pp. 1452–1458, 2024.
- [5] K. Schindler and D. Suter, "Object detection by global contour shape," Pattern Recognit., vol. 41, pp. 3736-3748, 2008.
- [6] G. Lee, M. Bajger, and M. Caon, "Multi-Organ Segmentation of CT Images using Statistical Region Merging," Proc. of the 9th IASTED International Conference on Biomedical Engineering (BioMed 2012), pp. 199-206, 2012.
- [7] X. Wang and J. Wu, "Remote sensing image segmentation based on statistical region merging and nonlinear diffusion," the 2nd Internat. Asia Conf. on Informatics in Control, Automation and Robotics (CAR 2010), pp. 32-35, 2010.
- [8] M. Howes, M. Bajger, G. Lee, F. Bucci, and S. Martelli, "Texture enhanced Statistical Region Merging with application to automatic knee bones segmentation from CT," 2021 Digital Image Computing: Techniques and Applications (DICTA), pp. 1-8, 2021.
- [9] D. Jeyakumari and D. Somasundareswari, "Blend color image segmentation of statistical region merging," Asian Journal of Information Technology, vol. 15, no. 4, pp. 765-771, 2016.
- [10] H. Zhang, W. Ni, W. Yan, H. Bian, and J. Wu, "Fast SAR image change detection using Bayesian approach based difference image and modified statistical region merging," The Scientific World Journal, vol. 2014, no. 1, pp. 1-12, 2014.
- [11] E. Aghabalaei, A. Ayatollahi, and M. R. Daliri, "Automatic lung nodule detection based on statistical region merging and support vector machines," Image Analysis & Stereology, vol. 36, no. 2, pp. 65-78, 2017.
- [12] Z. Huang, J. Zhang, X. Li, and H. Zhang, "Remote sensing image segmentation based on Dynamic Statistical Region Merging," Optik, vol. 125, no. 2, pp. 870-875, 2014.
- [13] A. Yabushita and K. Ogawa, "Image reconstruction with a hexagonal grid," In: IEEE Nuclear Science Symposium Conf. Record, vol. 3, pp. 1500-1503, 2002.
- [14] L. Middleton and J. Sivaswamy, "Hexagonal Image Processing: A Practical Approach," 1st ed., ser. Advances in Computer Vision and Pattern Recognition. Springer Science & Business, 2005.
- [15] M. Knaup, S. Steckmann, O. Bockenbach, and M. Kachelriess, "Image reconstruction using hexagonal grids," In: IEEE Nuclear Science Symposium Conf. Record, pp. 3074-3076, 2007.
- [16] K. Mueller and F. Xu, "Optimal Sampling Lattices for High-Fidelity CT Reconstruction," In: IEEE Medical Imaging Conf. Record, pp. 1-5, 2009.
- [17] Y. Wei, X. Li, J. Wang, C. Zhang, and Y. Liu, "Graph cuts image segmentation in a hexagonal image processing framework," J. Computational Information Systems, vol. 8, no. 14, pp. 5953-5960, 2012.
- [18] T. Schlosser, M. Friedrich, and D. Kowerko, "Hexagonal Image Processing in the Context of Machine Learning: Conception of a Biologically Inspired Hexagonal Deep Learning Framework," in the 18th IEEE Internat. Conf. on Machine Learning and Appl. (ICMLA), 2019.
- [19] X. Zheng, "Some efficient algorithms for morphological operations on hexagonal lattices and regular hexagonal domains," Proc. SPIE, vol. 11584, pp. 115840B-1–9, 2020.
- [20] X. Zheng, "Computer simulations for the denoising effect of morphological reconstructions for CT images on hexagonal grids and regular hexagonal regions," Proc. SPIE, vol. 12076, pp. 120760G-1–12, 2021.
- [21] X. Zheng, "Rectangular body-centered cuboid packing lattices and their possible applications," Journal of Computer Science Research, vol. 1, no. 2, pp. 1–7, 2019.
- [22] Y. Y. Boykov and M. -P. Jolly, "Interactive graph cuts for optimal boundary & region segmentation of objects in N-D images," Proc. 8th IEEE Internat. Conf. on Computer Vis. (ICCV 2001), pp. 105–112, 2001.

- [23] P. Felzenszwalb, D. Huttenlocher, "Efficient Graph-Based Image Segmentation," International Journal of Computer Vision, vol. 59, no. 2, pp. 167–181, 2004.
- [24] C. Sasi varnan, A. Jagan, J. Kaur, D. Jyoti, and D.S. Rao, "Image quality assessment techniques in spatial domain," Int. J. Comput. Sci. Technol., vol. 2, no. 3, pp. 177-184, 2011.
- [25] Rob J. Hyndman, "Another Look at Forecast Accuracy Metrics for Intermittent Demand," Foresight: The International Journal of Applied Forecasting, vol. 4, pp. 43–46, 2006.
- [26] H. K. Mittal, A. C. Pandey, M. Saraswat, S. Kumar, R. Pal, and G. Modwel, "A comprehensive survey of image segmentation: clustering methods, performance parameters, and benchmark datasets," Multimedia Tools and Applications, pp. 1–26, 2021.
- [27] N. Seo, "Normalized Cuts and Image Segmentation," http://note.sonots.com
- [28] Radiopaedia, "The first frame of Coronal postcontrast images for solitary fibrous tumors," https://radiopaedia.org/articles/solitary-fibrous-tumour
- [29] W. Khan, "Image Segmentation Techniques: A Survey," Journal of Image and Graphics, vol. 1, no. 4, pp. 166–170, 2013.
- [30] N. Richard, C. Fernandez-Maloigne, C. Bonanomi, and A. Rizzi, "Fuzzy Color Image Segmentation using Watershed Transform," Journal of Image and Graphics, vol. 1, no. 3, pp. 157–160, 2013.
- [31] R. Kaur and Er. Garima Malik, "An Image Segmentation Using Improved FCM Watershed Algorithm and DBMF," Journal of Image and Graphics, vol. 2, no. 2, pp. 106–112, 2014.
- [32] K. K. Thanammal, J. S. Jayasudha, R. R. Vijayalakshmi, and S. Arumugaperumal, "Effective Histogram Thresholding Techniques for Natural Images Using Segmentation," Journal of Image and Graphics, vol. 2, no. 2, pp. 113–116, 2014.
- [33] X. Zheng and F. Gu, "Fast Fourier transform on FCC and BCC lattices with outputs on FCC and BCC lattices respectively," J. Math. Imaging Vis., vol. 49, no. 3, pp. 530–550, 2014.